Highly-charged-ion-induced electron emission from C_{60} thin films

E. Bodewits and R. Hoekstra*
KVI-Atomic and Molecular Physics, University of Groningen, Zernikelaan 25, NL-9747 AA Groningen, The Netherlands

G. Kowarik, K. Dobes, and F. Aumayr
Institute of Applied Physics, TU Wien-Vienna University of Technology, A-1040 Vienna, Austria

(Received 11 August 2011; published 24 October 2011)

The secondary electron yields as a result of highly charged ions impinging on clean Au(111) and thin films of C_{60} on Au have been measured. This has been done for film thicknesses of one to five monolayers and several charge states of Ar and Xe ions. For all ions an increase of 35% in the secondary electron yield is observed when going from Au(111) to multiple C_{60} layers. The increase remains constant for a wide range (7–26) of charge states. Possible scenarios are given to explain the increase in electron yield.

DOI: 10.1103/PhysRevA.84.042901 PACS number(s): 79.20.Rf, 34.70.+e

I. INTRODUCTION

Ever since the advent of sources for highly charged ions (HCIs) the interaction of these ions with surfaces has been a field of very active research. One of the main interests is understanding the fundamental processes by which the large amounts of potential energy carried by the HCIs are dissipated at a surface within very short interaction times. For example the potential energy of an Ar^{13+} ion is already no less than 3.3 keV. The general trends of neutralization and relaxation mechanisms of such HCIs interacting with a surface are described by the hollow-atom scenario [1–5]. A key ingredient in this scenario is the electronic structure [2,6–9] of the surface and especially the work function. A possible way to tune the work function of a surface is by means of thin-film deposition. In this work C_{60} deposition on a Au(111) sample has been used to change the surface electronic structure.

Until now only a few pioneering experiments on hollow-atom formation at thin films have been done. The Oak Ridge group (Meyer *et al.* [7]) used Cs films on Au(011) to lower gradually the work function from Au(011) by 3.3 eV. They observed an increase in the *KLL* Auger electron yield when the work function of Au was lowered. The increase of above-surface *KLL* electron emission is explained by the larger distance in front of the surface at which the highly charged ions start capturing electrons. This implies an extended time that is available for hollow-atom decay, which is even further enhanced due to a reduced image charge acceleration.

The Groningen group (Khemliche *et al.* [6,10,11]) measured *KLL* electrons from O^{7+} and N^{6+} ions interacting with a LiF-covered Au target. In contrast to Cs, LiF deposition increases the binding energies of the surface electrons. However, for a single monolayer of LiF on Au, the total *KLL* Auger intensity did not change for O^{7+} and even increased by nearly 30% for N^{6+} ions. In a successive experiment Laulhé *et al.* [8] evaporated one-monolayer (ML) C_{60} films on Au to study changes in the *KLL* Auger electron spectra of the hydrogenlike N and O ions. From the shape of the *KLL* spectra it appeared that the filling of the *L* shell happens very efficiently on a C_{60} film while just as for LiF the binding energy of the least-bound surface electrons is increased by evaporating C_{60} on Au.

The *KLL* Auger decays represent (one of) the last steps in the relaxation of the hollow atoms. The initial steps in which low-energy electrons are emitted should be influenced more directly by work function changes. Low-energy electrons form the by far largest fraction of all electrons emitted. Therefore, we determined total secondary electron yields for highly charged Ar^{q+} (with $q = 7$–13) and Xe^{q+} (with $q = 10$–26) ions impinging on thin films of C_{60} deposited on Au. The film thickness was changed from zero to five MLs. Over this thickness range the electronic structure of the surface changes from Au-like to bulk C_{60} [12]. In this way the work function is gradually changed from 5.3 to 7.5 eV, i.e., from metallic to semiconducting and insulating.

In plasma-wall interactions the sheath potential is an important parameter. The sheath potential is influenced by particle-induced secondary electron emission [13]. In most present-day thermonuclear reactors the plasma-facing walls get covered by porous, flaky layers of graphite. C_{60} films with their open structure may be used to get an indication of the effect of those graphite layers on particle-induced secondary electron emission.

II. EXPERIMENTAL SETUP

The experiments have been performed in the experimental setup of IISIS (Inelastic Ion Surface Interaction Station), which is constructed to be used as a user station at the HITRAP facility at the Helmholtz Zentrum GSI (Darmstadt, Germany) [14,15]. The experimental setup of IISIS consists of a central CF-150 UHV chamber and is schematically depicted in Fig. 1. The base pressure in the main chamber is in the 10^{-11} mbar regime and kept there by means of a 400-l/s ion pump. During the measurements the pressure is in the 10^{-10} regime and kept there by a 360-l/s turbo pump while the ion pump is switched off in order not to interfere with the secondary electron measurements.

The ions are transported through a set of diaphragms and interact with the sample mounted on a VG Scienta manipulator equipped with a home-built sample holder. The present design of the sample holder ensures that the ion beam does not interact

*hoekstra@kvi.nl

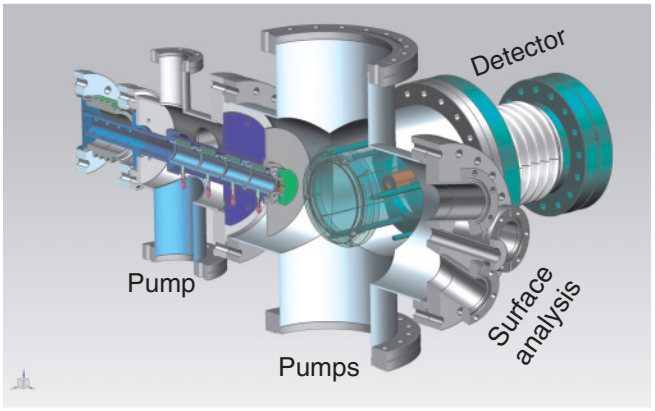

FIG. 1. (Color online) Schematic view of the experimental setup. Indicated are the manipulator (top), pumps (differential pumping left side, main pumps of the chamber below the main chamber), and surface analysis tools. Also the diaphragms and lenses are shown, as well as the surface barrier detector and the grid in front of it. For further details see text.

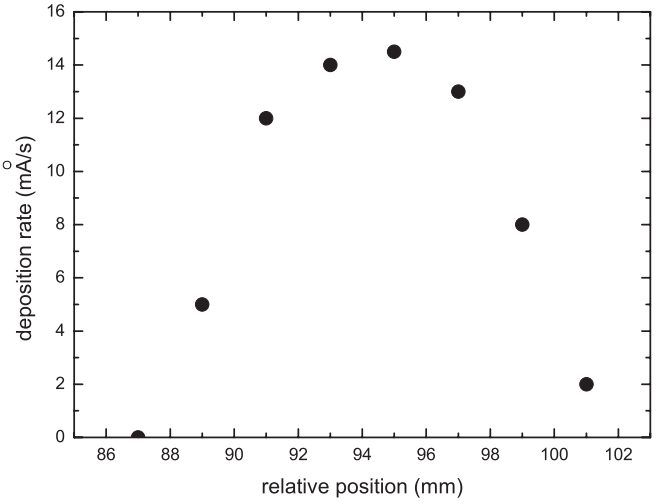

FIG. 2. The deposition rate vs relative position on the translation stage: the beam profile shows that the sample (8 × 5.5 mm) is fully covered by C_{60}.

with the support material. The sample can be rotated over 360° and moved in the X, Y, and Z directions.

The Au(111) target used in the present experiments is prepared by cycles of sputtering with 7-keV Ar^+ ions under grazing incidence angles and annealing at temperatures of up to 500 °C. The surface composition is checked by means of time-of-flight (TOF) low-energy ion scattering. The TOF system is mounted on the backside of the setup under an angle of 13° with respect to the incoming beam axis.

The electron statistics detector [16–18] is mounted under 90° with respect to the incoming beam. To collect all the emitted electrons on the electron statistics detector, the sample is surrounded by six electrodes. Five of the electrodes are biased negatively to optimize the electron collection efficiency. The sixth electrode, a highly transparent grid mounted directly in front of the electron statistics detector (see Fig. 1), is biased positively to attract electrons. The detector head is biased to 30 kV. This ensures the collection of all the emitted electrons. The electron number statistics detector itself is further described in [15,19,20] and references therein.

The deposition of thin films of C_{60} is done using an Omicron EFM 3 evaporator. The evaporator has a built-in flux monitor to monitor and control the outgoing particle flux. The evaporation of the C_{60} is done by means of electron-bombardment heating of a crucible containing C_{60} powder (99.9% pure, Sigma-Aldrich). In order to calibrate the deposition rate, a quartz microbalance (Tectra, type MTM-EK) is mounted on a linear translation stage, allowing to move the quartz crystal to the same position as where the sample is mounted during evaporation. Using the quartz microbalance, it is possible to measure deposited mass amounts equal to a small fraction of a monolayer.

The relation between deposited mass and layer thickness depends on a few parameters which can be captured in a proportionality factor, the so-called Z ratio. This Z ratio is defined by $\sqrt{d_q \mu_q / d_f \mu_f}$ where d_q and μ_q are the density and the shear modulus of the crystal (2.648 g/cm^3 and 29.5 GPa/cm^2, respectively) and d_f and μ_f the density (1.67 ± 0.02 g/cm^3 [21]) and shear modulus, respectively, of the deposited film. The shear modulus is given by $\mu = \frac{E}{2(1+\nu)}$ where E is Young's modulus and ν is the Poisson ratio which for C_{60} layers are 10 ± 2 GPa and 0.025 ± 0.08, respectively [21]. This gives a Z ratio of 3.4 ± 0.5.

To assess whether the sample gets fully and equally covered by C_{60}, the beam profile was measured by scanning the position of the quartz crystal through the C_{60} beam. Assuming that the beam has a Gaussian distribution, it can be seen in Fig. 2 that the FWHM of the evaporated C_{60} beam (8 mm) covers the full size of the Au(111) crystal (8 × 5.5 mm).

Before each deposition cycle, the deposition rate is monitored and it is made sure that the deposition rate is constant in time before the deposition cycle is started. When the deposition rate is constant, the quartz microbalance is retracted and the sample is moved to the same position as where the quartz crystal was located. Typical deposition rates are around one monolayer (7–8 Å) per 10 min. During and a short while after the evaporation (∼10 min), the sample is kept at an elevated temperature of 180 °C to ensure relaxation of the C_{60} on the surface.

III. RESULTS AND DISCUSSION

To study the effect of thin films on the hollow-atom dynamics we have deposited C_{60} films of 0–5 ML thickness on a Au sample. The effect of the films on the total electron yields has been studied for the impact of $7q$-keV Ar^{q+} ions (q = 7, 9, 11, 13) and 70-keV Xe^{q+} (q = 10, 12, 14, 16, 18, 20, 22, 24, 26) ions.

Figure 3 shows the total secondary electron yields γ obtained on the clean Au sample for an angle of incidence of 40° for Ar and 45° for Xe. These data serve as a reference to the results which have been obtained on the C_{60} films. The upper panel shows the secondary electron yield as a function of charge. As can been seen, the yields obtained with Ar^{q+} ions are larger when compared to the electron yield obtained with Xe^{q+} ions having the same charge state. In the lower panel, it can be seen that, replacing the charge by the potential energy

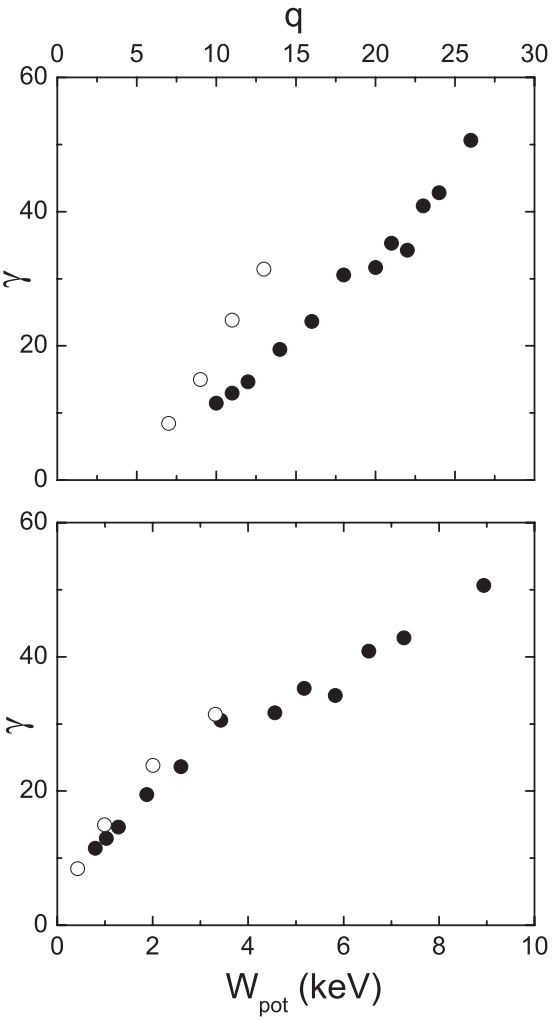

FIG. 3. Total electron yield for Ar^{q+} (open circles) and Xe^{q+} (closed circles) ion impact on clean Au(111) as a function of charge state (upper panel) and potential energy (lower panel) under incidence angles of 40° (Ar) and 45° (Xe), respectively.

of the ion, the yield obtained from Ar and Xe ions are very similar. This is a well-known fact [15,19,22–24] and relates to the electron emission being driven almost fully by the potential energy carried by the highly charged ions.

This implies that possible contributions due to kinetic electron emission are small. This is to be expected because of the relatively low kinetic energies of the ions. The Ar^{q+} ions have kinetic energies of 49 ($q = 7$) to 91 ($q = 13$) keV, which corresponds to velocities of (4.8–6.6) $\times 10^5$ m/s. These velocities are a bit above the threshold for kinetic electron emission on Au ($\sim 2.4 \times 10^5$ m/s [25]). On basis of the Ar^+ measurements by Eder *et al.* [25], one estimates a kinetic electron-emission contribution of at maximum 2 to 3 electrons. The Xe ions have a kinetic energy of 70 keV which corresponds to a velocity close to the kinetic emission threshold and thus kinetic electron emission is expected to be a very weak channel.

To compare the secondary electron yields γ obtained with the different ions on different thicknesses of the C_{60} layers, the

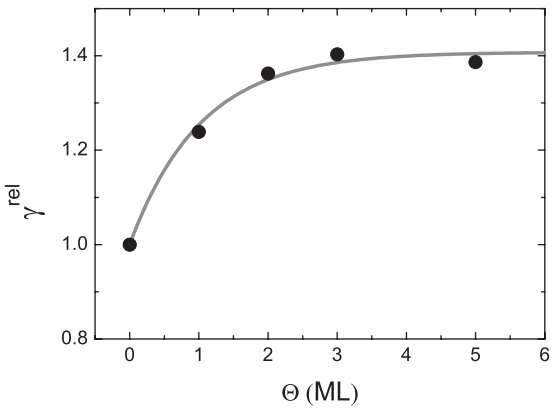

FIG. 4. Relative electron yield per incoming 70-keV Xe^{24+} ion impinging under an incidence angle of 40° on thin films of C_{60} of different layer thickness.

relative secondary electron yield, γ^{rel} is introduced:

$$\gamma^{\mathrm{rel}}(\Theta) = \frac{\gamma^{C_{60}}(\Theta)}{\gamma^{\mathrm{Au}}(\Theta = 0)}. \tag{1}$$

Here, $\gamma^{\mathrm{Au}}(\Theta = 0)$ is the secondary electron yield obtained on clean Au(111) (Fig. 3); $\gamma^{C_{60}}(\Theta)$ is the electron yield obtained on Θ monolayers of C_{60} deposited on the Au sample. As a typical example, Fig. 4 shows how the relative secondary electron yield of 91-keV Ar^{13+} impinging under an incidence angle of 40° changes as a function of the number of monolayers of C_{60} deposited on Au(111). The layers have been deposited sequentially; i.e., after deposition of the first monolayer the measurements have been performed after which another monolayer was deposited on top of the previous one. For a typical spectrum, 10^5 ions are more than sufficient. The surface area onto which these ions impinge is approximately 1 mm^2. Therefore, the damage to the thin film is negligibly small.

It can be readily seen that when layers of C_{60} are deposited on the Au(111) surface, the electron yield starts to increase. The largest increase in electron yield already occurs after deposition of the very first monolayer. At about five monolayers the increase saturates at a value of approximately 1.35 with respect to the clean gold. Also shown is a fit of an exponential gain curve, given by the equation

$$\gamma_{\mathrm{rel}}(\Theta) = \gamma_{\mathrm{rel}}^{\infty} - \left(\gamma_{\mathrm{rel}}^{\infty} - 1\right) e^{-\Theta/\Theta_{\mathrm{ch}}}. \tag{2}$$

with Θ the number of monolayers and $\gamma_{\mathrm{rel}}^{\infty}$ the relative yield for very thick layers, i.e., bulk C_{60}, and Θ_{ch} a characteristic layer thickness.

To investigate whether the relative increase in electron yield does depend on the charge state and thus the potential energy of the ion, similar series of experiments have been done with all the other highly charged Ar and Xe on up to five monolayers of C_{60}. The data were then fitted to Eq. (2) and the resulting values for $\gamma_{\mathrm{rel}}^{\infty}$ are shown in Fig. 5. For all highly charged ions the relative increase of the secondary electron yield is almost the same. The average value for $\gamma_{\mathrm{rel}}^{\infty}$ is found to be 1.35; i.e., the electron yield increases by 35% when going from a gold surface to a C_{60}-covered surface. Only for the lowest charge state used, Ar^{7+}, the increase is twice as high as the values for the other ions.

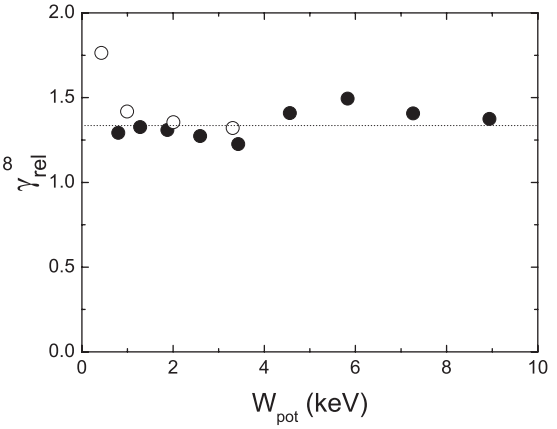

FIG. 5. The relative yield as a function of potential energy of Ar^{q+} (open circles) and Xe^{q+} (solid circles) impinging under 40° on C_{60}. The value of γ_{rel}^{∞} is obtained from Eq. (2).

At a first glance higher secondary electron yield for C_{60} as compared to Au seems counterintuitive since the binding energy of the electrons is roughly 2 eV larger than for the gold crystal. According to the over-the-barrier model [2,26], the distance in front of the surface at which first electron capture can occur is given (in atomic units) by

$$R_c = \frac{\sqrt{2q}}{E_b}\frac{\sqrt{\epsilon(7+\epsilon)}}{1+\epsilon}, \tag{3}$$

with E_b the binding energy of the least-bound target electrons, ϵ the dielectric constant, and q the ions' charge state. For a metal, $\epsilon = \infty$ and E_b corresponds to the work function of the metal. This implies that for C_{60} the first capture distance is shorter than for Au and thus there is less time available for relaxation of the hollow atoms by means of Auger decay before they penetrate the surface. In addition, because of the resonant nature of the electron capture, lower-lying, more strongly bound states in the hollow atom get populated which is likely to imply that fewer Auger steps are necessary for the full relaxation of the hollow atoms. On the basis of these arguments one is inclined to expect that fewer secondary electrons will be emitted for C_{60} than for Au. This expectation is in contrast to the experimental observations.

It is also unlikely that the existence of a band gap in bulk or thick films of C_{60} is driving the enhancement of secondary electron emission by prohibiting the common resonant electron loss from the hollow atom back into empty states of the surface just above the work function. At a film thickness of only one ML, already two-thirds of the increase in secondary electron yield is realized (cf. Fig. 4). From the data for all ions under study, the characteristic layer thickness Θ_{ch} is found to be 0.9 ± 0.3. From photoemission and atomic force microscopy studies [12,27–29] on one-ML C_{60} films on Au it is known that no full band gap has developed yet. Therefore, it seems likely that the presence of a band gap in bulk-like C_{60} does not play a very decisive role in the relaxation of the hollow atoms. This conclusion is in line with the one drawn by Khemliche *et al.* [6] for one ML of LiF on Au and which was based on the last steps of the hollow-atom decay, namely the *KLL* electron spectral intensities.

Recently the original over-the-barrier model was extended by Lake *et al.* [30] by the inclusion of a thin dielectric film on top of a metal surface. In their case the target system was Co covered with a 1.5-nm film of Al_2O_3. Lake and co-workers showed that a highly charged ion approaching the Al_2O_3 film may perturb the thin film such that throughout the film the bottom of its conduction band drops below the work function of the Co substrate while the barrier between the HCI and the thin film is still so high that over-the-barrier transitions between the film and the HCI are not yet possible. In this way the insulating aluminum oxide film effectively lowers the Co work function from approximately 5 to 3 eV. The earlier onset of the neutralization and creation of hollow atoms will give more time in front of the surface for the relaxation processes of the hollow atoms. This would lead to an increase in the secondary electron yields.

It is not straightforward to assess whether this scenario also holds for thin films of C_{60} on Au. Compared to aluminum oxide with a wide band gap of almost 10 eV, C_{60} has a rather narrow band gap of 2.5 eV only. This means that the difference between the work function of the Au sample and the top of the highest occupied molecular orbital of the C_{60} is small. But for C_{60} the bottom of the LUMO lies only approximately 0.5 eV above the work function of the Au sample, while for the Co-aluminum oxide system treated by Lake *et al.* this difference is about 1 eV. A further point to be considered is that for one-ML C_{60} films on Au no full band gap has developed yet, whereas for a single monolayer already the largest part of the increase in the secondary electron yields is realized.

There might be another cause for the increase in the secondary electron yield too, namely an increase in the escape length of electrons produced below the surface. The thin films of C_{60} have a very open structure; therefore, electrons produced in the C_{60} film may have a higher probability of escaping and being detected as compared to electrons produced below a closer-packed Au surface.

The effect of a different escape depth on secondary electron yields has been demonstrated for singly charged ions on a highly oriented pyrolytic graphite (HOPG) crystal [31]. Ions incident parallel to the graphite planes (open geometry) were shown to have secondary electron yields three times as high as for impact normal to the graphite planes.

The $7q$-keV Ar^{q+} ions and the 70-keV Xe^{q+} ions incident at 40° on a Au sample have a lateral penetration depth of 10 to 15 nm according to SRIM [32] simulations. Modeling the C_{60} film by a graphite layer of the same thickness and density, it is found that almost all projectiles pass through the C_{60} thin films (zero to five MLs). Therefore, the evaporation of a thin film with a large escape depth may lead to an increase in the secondary electron yield.

However, the *KLL* Auger spectra taken by Laulhé *et al.* for N^{6+} and O^{7+} ions impinging on one-ML C_{60} on Au hinted at a very fast, direct side-feeding, of the inner L shells. This would reduce the number of decay steps in the hollow-atom relaxation and the number of emitted electrons. Direct feeding from somewhat more strongly bound C_{60} levels creates vacancies in the C_{60} film that may be filled by subsequent Auger processes involving electrons from the conduction band of the metal substrate. This scenario was invoked by Matulevich *et al.* [33]

to describe the electron emission from Ar^+ ions interaction with a thin MgO film absorbed on a Mo substrate.

The secondary electron emission arising from the decay of hollow atoms created by the interaction of HCIs on a thin film is obviously determined by an intricate interplay of many processes. Given the experimental observation that for all highly charged Ar and Xe ions the secondary electron yield increases by 35%, the apparent lowering of the work function might be the main cause for the enhanced electron yield (model by Lake *et al*. [30]). To get more insight into the specific roles and strengths of these processes requires experiments with very low kinetic energy. This would allow for measuring electron yields of HCI which barely penetrate the surface. Also, changing the projectiles' kinetic energy gives the possibility to "tune" the time an ion spends in front of the surface.

It would also be interesting to use even higher charged ions in the same kinetic energy regime. In the (near) future access to these slow, very highly charged ions will be provided by HITRAP at GSI [12].

IV. CONCLUSIONS

The secondary electron yields from highly charged Ar and Xe ions impinging on Au(111) and thin films of C_{60} evaporated on Au(111) have been determined. In order to quantify and compare the results obtained for Ar and Xe ions in a wide range of charge states, the relative yield γ^{rel} has been introduced. When thin films of C_{60} are evaporated on the Au sample, the secondary electron yield increases. The increase saturates at approximately 35%, when five monolayers are evaporated on the surface. The increase in electron yield as a function of film thickness is well described by an exponential gain function and is virtually constant when ions are used that carry a potential energy between 0.5 and 10 keV.

Several possible causes which may explain the observed increase in secondary electron yield have been considered. It is clear that the stronger electron binding energy and band gap of thick C_{60} films are not responsible for the increase in secondary electron yields. The open structure of the thin films of C_{60} molecules is likely to lead to an increase of secondary electron yields, since the films have an increased mean escape depth of the electrons created inside the target system. A possible second and maybe more likely explanation could be that the interplay between the Coulombic field of the highly charged ion and the electronic structure of the thin film leads to an apparent, effective lowering of the work function of the system (Lake *et al*. [30]). The first possibility is driven by projectile ions penetrating the thin films while the second one deals with ions in front of the surface. Future experiments at much lower energy at which the projectile ions barely penetrate the surface may help to resolve the specific contributions to the observed increase in secondary electron yields.

ACKNOWLEDGMENTS

This experiment has been performed at the ZERNIKELEIF part of the distributed LEIF infrastructure. Support received by the European Project ITS LEIF (Grant No. RII3/026015) is gratefully acknowledged. This work is also sponsored by the Helmholtzzentrum für Schwerionenforschung GmbH (GSI), Germany-KVI University of Groningen collaboration agreement and the FOM-EURATOM association agreement. The "Stichting voor Fundamenteel Onderzoek der Materie" (FOM) is financially supported by the "Nederlandse organisatie voor Wetenschappelijk Onderzoek" (NWO). The Austrian part of the work has been supported by the Austrian Science Foundation FWF, by the Association EURATOM-ÖAW, and by the Kommission zur Koordination der Kernfusionsforschung in Österreich KKKÖ.

[1] A. Arnau *et al*., Surf. Sci. Rep. **27**, 113 (1997).
[2] J. Burgdörfer, P. Lerner, and F. W. Meyer, Phys. Rev. A **44**, 5674 (1991).
[3] H. P. Winter and F. Aumayr, J. Phys. B **32**, R39 (1999).
[4] J. Thomaschewski, J. Bleck-Neuhaus, M. Grether, A. Spieler, and N. Stolterfoht, Phys. Rev. A **57**, 3665 (1998).
[5] F. Aumayr and H. P. Winter, Springer Tracts Mod. Phys. **225**, 79 (2007).
[6] H. Khemliche, T. Schlathölter, R. Hoekstra, R. Morgenstern, and S. Schippers, Phys. Rev. Lett. **81**, 1219 (1998).
[7] F. W. Meyer, L. Folkerts, I. G. Hughes, S. H. Overbury, D. M. Zehner, P. A. Zeijlmans van Emmichoven, and J. Burgdörfer, Phys. Rev. A **48**, 4479 (1993).
[8] C. Laulhé, R. Hoekstra, S. Hoekstra, H. Khemliche, R. Morgenstern, A. Närmann, and T. Schlathölter, Nucl. Instrum. Methods B **157**, 304 (1999).
[9] M. Unipan, A. Robin, R. Morgenstern, and R. Hoekstra, Phys. Rev. Lett. **96**, 177601 (2006).
[10] H. Khemliche, T. Schlathölter, R. Hoekstra, and R. Morgenstern, Phys. Rev. A **60**, 3800 (1999).
[11] H. Khemliche, C. Laulhé, S. Hoekstra, R. Hoekstra, and R. Morgenstern, Phys. Scr., T **80**, 66 (1999).
[12] A. J. Maxwell, P. A. Brühwiler, A. Nilsson, N. Mårtensson, and P. Rudolf, Phys. Rev. B **49**, 10717 (1994).
[13] N. Schupfer, D. D. Tskhakaya sr, R. Khanal, S. Kuhn, F. Aumayr, S. F. da Silva, and W. HP, Plasma Phys. Controlled Fusion **48**, 1093 (2006).
[14] T. Beier, L. Dahl, H.-J. Kluge, C. Kozhuharov, and W. Quint, Nucl. Instrum. Methods B **235**, 473 (2005).
[15] E. Bodewits, H. Bekker, A. J. de Nijs, R. Hoekstra, D. Winklehner, B. Daniel, G. Kowarik, K. Dobes, and F. Aumayr, Nucl. Instrum. Methods B **269**, 1203 (2011).
[16] G. Lakits, F. Aumayr, and H. P. Winter, Rev. Sci. Instrum. **60**, 3151 (1989).
[17] K. Töglhofer, F. Aumayr, and H. P. Winter, Surf. Sci. **281**, 143 (1993).
[18] H. Eder, M. Vana, F. Aumayr, and H. P. Winter, Rev. Sci. Instrum. **68**, 165 (1997).
[19] W. Meissl, D. Winklehner, F. Aumayr, M. C. Simon, R. Ginzel, J. R. C. López-Urrutia, J. Ullrich, B. Solleder, C. Lemell, and J. Burgdörfer, e-J. Surf. Sci. Nanotechnol. **6**, 184 (2008).
[20] C. Lemell, J. Stockl, H. P. Winter, and F. Aumayr, Rev. Sci. Instrum. **70**, 1653 (1999).

[21] A. A. Kolomenskii, M. Szabadi, and P. Hess, Appl. Surf. Sci. **86**, 591 (1995).
[22] H. Kurz, F. Aumayr, C. Lemell, K. Töglhofer, and H. P. Winter, Phys. Rev. A **48**, 2182 (1993).
[23] J. Wang, J. Zhang, J. Gu, X. Luo, and B. Hu, Phys. Rev. A **80**, 062902 (2009).
[24] W. Meissl, M. Simon, J. C. López-Urrutia, H. Tawara, J. Ullrich, H. P. Winter, and F. Aumayr, Nucl. Instrum. Methods B **256**, 520 (2007).
[25] H. Eder, F. Aumayr, and H. P. Winter, Nucl. Instrum. Methods B **154**, 185 (1999).
[26] A. Bárány and C. J. Setterlind, Nucl. Instrum. Methods B **98**, 184 (1995).
[27] I. F. Torrente, K. J. Franke, and J. I. Pascual, J. Phys. Condens. Matter **20**, 184001 (2008).
[28] F. Schiller, M. Ruiz-Osés, J. E. Ortega, P. Segovia, J. Martínez-Blanco, B. P. Doyle, V. Pérez-Dieste, J. Lobo, N. Néel, R. Berndt, and J. Kröger, J. Chem. Phys. **125**, 144719 (2006).
[29] M. Hinterstein, X. Torrelles, R. Felici, J. Rius, M. Huang, S. Fabris, H. Fuess, and M. Pedio, Phys. Rev. B **77**, 153412 (2008).
[30] R. E. Lake, J. M. Pomeroy, and C. E. Sosolik, Nucl. Instrum. Methods B **269**, 1199 (2011).
[31] S. Cernusca, M. Fürsatz, H. P. Winter, and F. Aumayr, Europhys. Lett. **70**, 768 (2005).
[32] J. Ziegler, J. Biersack, and M. Ziegler, The Stopping and Range of Ions in Matter (SRIM) (Lulu Press Co., Morrisville, NC, USA, 2008).
[33] Y. T. Matulevich and P. A. Zeijlmans van Emmichoven, Phys. Rev. B **69**, 245414 (2004).